

3) Did I miss it -  $\delta\chi^2$  for young/old w Gaussian vs asymmetric Gaussian?

- 1) Current SNeIa  $N(z)$  does not look bimodal
- 2) What about Bayesian Hierarchical Models like UNITY + Steve?

## Redshift Evolution of the Underlying Type Ia Supernova Stretch Distribution

N. Nicolas \*<sup>1</sup>, M. Rigault \*\*<sup>2</sup>, R. Graziani<sup>2</sup>, Y. Copin<sup>1</sup>, M. Briday<sup>1</sup>, Y.-L. Kim<sup>1</sup>, and ...

<sup>1</sup> Université de Lyon, F-69622, Lyon, France; Université de Lyon 1, Villeurbanne; CNRS/IN2P3, Institut de Physique des Deux Infinis, Lyon

<sup>2</sup> Université Clermont Auvergne, CNRS/IN2P3, Laboratoire de Physique de Clermont, F-63000 Clermont-Ferrand, France.

Received 2 November 1992 / Accepted 7 January 1993

### ABSTRACT

The true nature of Type Ia supernovae (SNeIa) remains largely unknown and as measure as survey statistic increases, the question of astrophysical systematic uncertainties rises and notably that of the SNeIa population redshift drift. In this paper, we study the redshift evolution of SNeIa salt2.4 lightcurve stretches, which is a purely intrinsic SN property, to probe this drift. The SN stretch has been shown to strongly correlate with the SN's environment, and notably with stellar age tracers. Following the prediction of the fraction of young and old SNeIa in nature from Rigault et al. (2018), and assuming non-drifting underlying stretch distribution for each, we model the expected SNeIa stretch distribution as a function of redshift. We test our prediction against data from the literature selected to have negligible selection effects to ensure that any observed drift is indeed astrophysical and not artificial. We clearly demonstrate that the underlying SNeIa stretch distribution is evolving as a function of redshift and that the young/old drifting model is a much better description of the data than any non-drifting model, including the sample-based asymmetric distributions used by the Beams with Bias Correction Malmquist bias correction algorithm. Our favored underlying stretch model is bimodal: a high-stretch mode shared by both young and old environment and a low-stretch mode only existing in old environments. The underlying SNeIa population is evolving as a function of redshift and the exact impact on cosmology remains to be studied. Yet, the astrophysical drift of the SN stretch distribution does affect current Malmquist bias corrections and thereby distances derived from SN affected by selection effects. We highlight that such a bias will increase with surveys covering larger redshift ranges, which is particularly important for LSST.

**Key words.** Cosmology – Type Ia Supernova – Systematic uncertainties

### 1. Introduction

Type Ia supernovae (SNe Ia) are powerful cosmological distance indicators that have enabled the discovery of the acceleration of the Universe's expansion (Riess et al. 1998; Perlmutter et al. 1999). They remain today a key cosmological probe to understand the properties of dark energy (DE) as it is the only tool able to precisely map the recent expansion rate  $z < 0.5$ , when DE is driving it (e.g. Scolnic et al. 2019). They also are key to directly measure the Hubble Constant ( $H_0$ ), provided one can calibrate their absolute magnitude (Riess et al. 2016; Freedman et al. 2019). Interestingly, the value of  $H_0$  derived when the SNe Ia are anchored on Cepheids (the SH0ES project Riess et al. 2009, 2016) is  $\sim 5\sigma$  higher than what is predicted by cosmic microwave background (CMB) data measured by Planck assuming the standard  $\Lambda$ CDM, or when the SN luminosity is anchored at intermediate redshift by the baryon acoustic oscillation (BAO) scale (Riess et al. 2019; Reid et al. 2019; Planck Collaboration et al. 2016; Feeney et al. 2019). While using the tip of the red giant branch technique in place of the Cepheids seem to favor an intermediate value of  $H_0$  (Freedman et al. 2019, 2020), time delay measurements from strong lensing seem to also favor high  $H_0$  values (Wong et al. 2019).

The  $H_0$  tension has received a lot of attention as it could be a sign of new fundamental physics. Yet, no simple solution is able to accommodate this  $H_0$  tension when accounting for all

other probes (Knox & Millea 2019) and the current most promising scenario appears to be a burst of expansion at the matter-radiation decoupling moment caused by a (fine tuned) early dark energy (Poulin et al. 2019).

Alternatively, systematic effects affecting one or several of the aforementioned analysis could also explain the tension. In Rigault et al. (2015) we suggested that SNe Ia from the Cepheid calibrator sample differs by construction from the Hubble flow as it strongly favors young stellar population environments where one could find Cepheids. This selection effect would impact the derivation of  $H_0$  if SNe Ia from young and older environments differ in average magnitudes.

For the last decades, numerous analysis have studied the relation between SNe Ia and host properties, finding first that the standardized SNe Ia magnitude significantly depends on the host stellar-mass, SNe Ia from high-mass host being brighter on average (e.g. Kelly et al. 2010; Sullivan et al. 2010; Childress et al. 2013; Betoule et al. 2014; Rigault et al. 2018; Kim et al. 2019). This mass-step correction is currently used in cosmological analyses (e.g. Betoule et al. 2014; Scolnic et al. 2018), including for deriving  $H_0$  (Riess et al. 2016, 2019). Yet, the underlying connection between the SN and the host remains unclear when using global properties such as the host stellar mass, which raises the question of the accuracy of the correction. More recently, studies have used the local SN environment to probe more direct connections between the SN and its environments (Rigault et al. 2013), showing that local age-tracers such as the local specific star formation rate or the local color are more strongly correlated with

\* n.nicolas@ipnl.in2p3.fr, equal contribution

\*\* m.rigault@ipnl.in2p3.fr, equal contribution

the standardized SN magnitude (Rigault et al. 2018; Roman et al. 2018; Kim et al. 2018), suggesting the age to be the driving parameter underlying the mass-step. If true, this would have a significant impact for cosmology because the redshift drift magnitude correction to apply might strongly vary (Rigault et al. 2013; Childress et al. 2014; Scolnic et al. 2018). Yet, the importance of local SN environmental study remains highly debated (e.g. Jones et al. 2015, 2019) and especially the impact it has on the derivation of  $H_0$  (Jones et al. 2015; Riess et al. 2016, 2018; Rose et al. 2019).

In this paper, we take a step aside to probe the validity of our modeling of the SN population that we claim to be constituted of two age populations (Rigault et al. 2013; Rigault et al. 2015, 2018): one old and one young, the former having on average lower lightcurve stretches and being brighter after standardization. We indeed use the correlation between the SN age probed with local specific star formation rate in Rigault et al. (2018) and the SN stretch to model the expected evolution of the underlying SN stretch distribution as a function of redshift. This modeling relies on three assumptions: (1) there are indeed two populations of SNe Ia; (2) the relative fraction of each of these populations as a function of redshift follows the age-modeling made in Rigault et al. 2018; and (3) the underlying distribution of stretch for each age-sample can be modeled and do not significantly drift. This paper aims at testing this with datasets from the literature.

The concept of the SNe Ia age dichotomy aroused when the SN Ia rate has first been studied. Mannucci et al. (2005); Scannapieco & Bildsten (2005); Sullivan et al. (2006); Aubourg et al. (2008) have shown that the relative SNe Ia rate in galaxies could only be explained if two populations existed, one young, following the host star formation activity, and one old following the host stellar mass (the so called "prompt and delayed" or "A+B" model). In Rigault et al. (2018) we used the specific Star Formation Rate at the SN location (Local sSFR or LsSFR) to classify which are the prompts (those with a high LsSFR) and which are the delayed (those with low LsSFR). Furthermore, since the first SNe Ia host analysis, the SN stretch has been known to be strongly correlated with the SN host properties (Hamuy et al. 1996, 2000), which has been extensively confirmed since (e.g.Neill et al. 2009; Sullivan et al. 2010; Lampeitl et al. 2010; Kelly et al. 2010; Gupta et al. 2011; D'Andrea et al. 2011; Childress et al. 2013; Rigault et al. 2013; Pan et al. 2014; Kim et al. 2019). Following the "A+B" model and the connection between SN stretch and host properties, Howell et al. (2007) first discussed the potential redshift drift of the SN stretch distribution. In this paper we revisit this analysis with the most recent SNe Ia dataset.

We present in section 2 the sample we are using for this analysis, which is based on the Pantheon dataset (Scolnic et al. 2018). We discuss the importance of obtaining a "complete" sample, i.e. representative of the true underlying SNe Ia distribution, and how we build one from the Pantheon sample. We then present in section 3 our modeling of the distribution of stretch as a function of redshift based on stretch distribution of young and old SNe Ia. Our results are presented in section 4, where we test if the SN stretch does evolve as a function of redshift and if the age model is in good agreement with this evolution. Consequence for cosmology of our results are briefly discussed in section 5.2 and we conclude in section 6.

## 2. Complete Sample Construction

We base our analysis on the latest SNe Ia compilation: the Pantheon catalog from Scolnic et al. (2018). A naive approach to test the SN stretch redshift drift would be to simply compare the

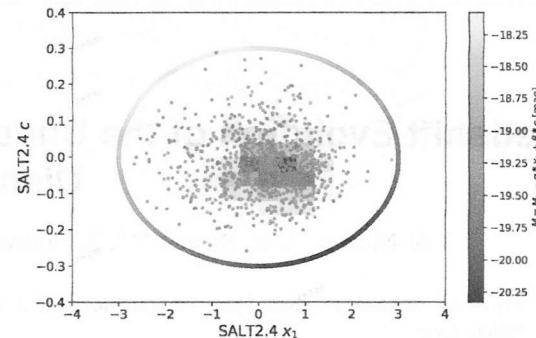


**Fig. 1.** SALT2.4 stretch ( $x_1$ ) and color ( $c$ ) lightcurve parameters of SNe Ia from the SDSS, PS1 and SNLS samples from the Pantheon catalog. The individual SNe are shown as blue dots and a 2D histogram is shown in gray to highlight point density. The ellipse ( $x_1 = \pm 3, c = \pm 0.3$ ) is displayed, colored by the corresponding standardized absolute magnitude using the  $\alpha$  and  $\beta$  coefficients from Scolnic et al. (2018). The grey diagonal lines represent the  $(x_1, c)$  evolution for  $m = m_{lim}$ , for  $z$  between 0.50 and  $z = 1.70$  using SNLS's  $m_{lim}$  of 24.8 mag.

with redshift

observed SN stretch distributions in a few bins of redshift. In practice, selection effects are affecting the observed SN stretch distributions. Indeed, because the observed SN Ia magnitude correlates with the lightcurve stretch (and color), the first SN Ia that a magnitude-limited survey will miss are the lowest-stretch (and reddest) ones. Consequently, if selection effects are not accounted for, one might confuse true population drift with selection effects, and conversely.

Assuming sufficient (and unbiased) spectroscopic follow-up for acquiring typing and host redshift, the selection effects of magnitude-limited surveys should be negligible below a given redshift where even the faintest SNIa can be observed. In contrast, targeted surveys have highly complex selection functions and will be discarded from our analysis. Fortunately, modern SN cosmology samples such as the Pantheon dataset are now dominated by magnitude limited surveys.

We present in Fig. 1 the lightcurve stretch and color distributions of SNe Ia from the following surveys: PanStarrs (PS1 Rest et al. 2014), the Sloan Digital Sky Survey (SDSS Frieman et al. 2008) and the SuperNovae Legacy Survey (SNLS Astier et al. 2006). An ellipse in the SALT2.4 ( $x_1, c$ ) plane with  $x_1 = \pm 3$  and  $c = \pm 0.3$  encapsulates the full distribution (Guy et al. 2007; Betoule et al. 2014); see also Bazin et al. (2011) and Campbell et al. (2013) for similar contours, the second using a more conservative  $|c| \leq 0.2$  cut. Assuming the SN absolute magnitude with  $x_1 = 0$  and  $c = 0$  is  $M_0 = -19.36$  (Kessler et al. 2009; Scolnic et al. 2014), we can derive the absolute standardized magnitude at maximum of light  $M = M_0 - \alpha x_1 + \beta c$  along the aforementioned ellipse given the standardization coefficient  $\alpha = 0.156$  and  $\beta = 3.14$  from Scolnic et al. (2018): the faintest SN Ia is that with  $(x_1 = -1.66, c = 0.25)$  and an absolute standardized magnitude at peak in Bessel-B band of  $M_{lim}^{fo} = -18.31$  mag. Since one needs to detect this object typically a week before and 10 days after peak to build a suitable lightcurve, the limiting standardized absolute magnitude effectively is approximately  $M_{lim} = -18.00$  mag. Hence, given the magnitude limit  $m_{lim}$  of a magnitude limited survey, one can derive the maximum redshift  $z_{lim}$  above which the faintest SNe Ia will be missed using the relation between apparent magnitude, redshift and absolute magnitude  $\mu(z_{lim}) = m_{lim} - M_{lim}$ .

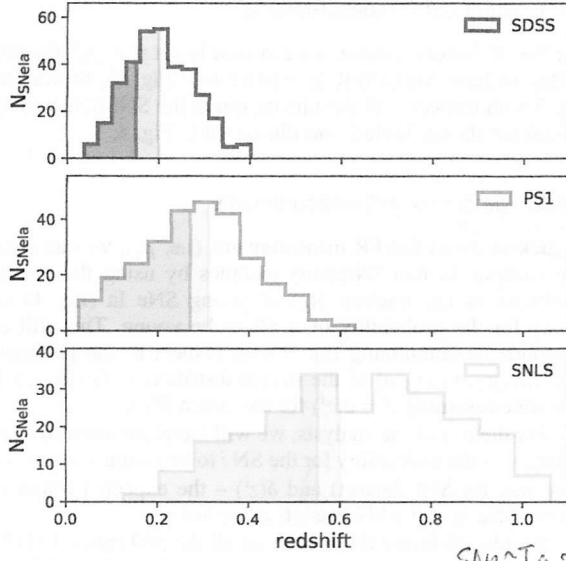


**Fig. 2.** From top to bottom: Redshift histograms of SNe Ia from the SDSS, PS1 and SNLS dataset respectively (data from Pantheon Scolnic et al. 2018). The colored parts represent the distribution of SNe Ia kept in our analysis for they are supposedly free from selection bias (see section 2). The dark (resp. light) color responds to the conservative (resp. fiducial) selection cut.

SNLS typically acquires SNe Ia in the redshift range  $0.4 < z < 0.8$ . At these redshifts the rest-frame Bessel-B band roughly corresponds to the SNLS-*i* filter that has a  $5\sigma$  depth of 24.8 mag<sup>1</sup>. This converts to a  $z_{lim} = 0.60$ , in perfect agreement with Neill et al. (2006), Perrett et al. (2010) and Bazin et al. (2011). Fig. 14 of Perrett et al. 2010 suggests a lower limit of  $z_{lim} = 0.55$ ; both will be considered as discussed below.

Similarly, PS1 observes SNe Ia in the range  $0.2 < z < 0.4$ , their *g*-band  $5\sigma$  depth is 23.1 mag (Rest et al. 2014), which yields to  $z_{lim} = 0.30$  in agreement with, e.g., Fig. 6 of Scolnic et al. (2018). This figure could also suggest a more conservative  $z_{lim}$  of 0.27.

In similar redshift range, SDSS has a limiting magnitude of 22.5 (Dilday et al. 2008; Sako et al. 2008), which would lead to a  $z_{lim} = 0.24$ . However, the SDSS surveys were more sensitive to limited spectroscopic resources. Kessler et al. (2009) pointed out that during year-1 of SDSS, SNe Ia with *r-mag*  $< 20.5$  were favored for spectroscopic follow up, corresponding to a redshift cut at 0.15. For the rest of the SDSS survey, additional spectroscopic resources were used, and Kessler et al. (2009) and Dilday et al. (2008) show a relative completeness up to  $z_{lim} = 0.2$ . Following these analyses we will use  $z_{lim} = 0.2$  as the baseline SDSS redshift limit.

For the rest of the analysis, we will consider the aforementioned redshift limits as well as more conservative cuts for each of these surveys, namely  $z_{lim} = 0.15$  for SDSS,  $z_{lim} = 0.27$  for PS1 and  $z_{lim} = 0.55$  for SNLS.

The complete sample selection is summarized in Table 1, and the redshift distribution of these three surveys are shown in Fig. 2. As expected, the selected redshift limits roughly correspond to the peak of these histograms.

In addition, we use the SNe Ia from the Nearby Supernova Factory (SNfactory, Aldering et al. 2004) published in Rigault

**Table 1.** Composition of the SNe Ia dataset used in this analysis. Conservative cuts are indicated in brackets.

Survey	$z_{lim}$	$N_{SN}$
SNf	–	114
SDSS	0.20(0.15)	167(82)
PS1	0.30(0.27)	160(122)
SNLS	0.60(0.55)	102(78)
HST	–	26
Total	–	569(422)

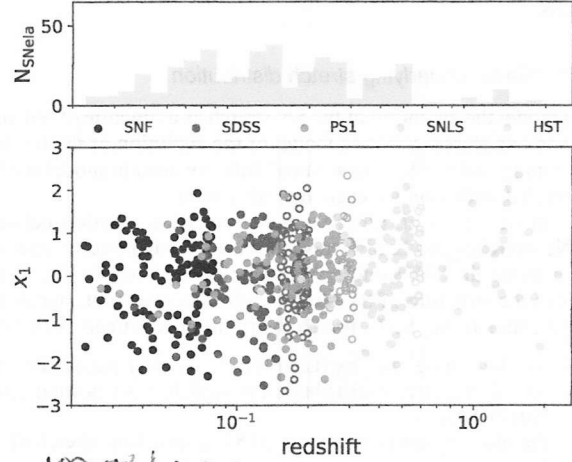


**Fig. 3.** *Main:* SALT2.4 lightcurve stretch as a function of redshift (in log) for each survey considered in this analysis (see legend). Full (resp. empty) markers correspond to the conservative (resp. fiducial) selection cuts. *Top:* combined redshift histogram in dark (resp. light) gray for the conservative (resp. fiducial) selection cuts.

et al. (2018) and have been discovered from non-targeted searches (114 SNe Ia, see their section 3 and 4.2.2). Their spectroscopic follow-up were done on a redshift range of  $0.02 < z < 0.09$  (as in Rigault et al. 2018), while the searches were much deeper. As such, these SNe Ia should also be a random sampling of the underlying SN population. The SNf sample is particularly useful for studying SN property drift as it enables us to have a large SN Ia sample at  $z < 0.1$ .

Finally, we included the HST sample from Pantheon, that follows the same logic of having a search deeper than the follow-up and we therefore kept it entirely (Strolger et al. 2004), see Table 1. We present the stretch distribution and redshift histogram of these five surveys in Fig. 3.

### 3. Modeling the redshift drift

In Rigault et al. (2018) we presented a modeling of the evolution of the fraction of prompt and delayed SNe Ia as a function of redshift following former work on rates and delay time distributions (e.g., Mannucci et al. 2005; Scannapieco & Bildsten 2005; Sullivan et al. 2006; Aubourg et al. 2008; Childress et al. 2014; Maoz et al. 2014). In short, we assumed that the number of prompt SNe Ia follows the star formation activity (SFR) in the Universe while the number of delayed SNe Ia follows the number of Gyr-old stars in the Universe, i.e. the stellar mass ( $M^*$ ).

<sup>1</sup> CFHT final release website.

Hence, if we denote  $\delta(z)$  (resp.  $\psi(z) = 1 - \delta(z)$ ) the fraction of young (resp. old) SNe Ia in the Universe as a function of redshift, then their ratio  $\delta/\psi$  is expected to follow the evolution of the specific star formation rate (SFR/M\*) which goes as  $(1+z)^{2.8}$  until  $z \sim 2$  (e.g., Tasca et al. 2015). Since  $\delta(0.05) \sim \psi(0.05)$  (Rigault et al. 2013; Rigault et al. 2018; Wiseman et al. 2020), in agreement with rate expectations (Mannucci et al. 2006; Rodney et al. 2014), we conclude in Rigault et al. (2018) that

$$\delta(z) = (K^{-1} \times (1+z)^{-2.8} + 1)^{-1} \quad (1)$$

with  $K = 0.87$ . This model is comparable to the evolution predicted by Childress et al. (2014) based on SN rates in galaxies depending on their quenching time as a function of their stellar mass.

### 3.1. "Base" underlying stretch distribution

To model the evolution of the SN stretch as a function of redshift, given our aforementioned model of the evolution of the fraction of young and old SNe Ia with redshift, we need to model the SN stretch distribution for each age subsample.

In Rigault et al. (2018), we presented the relation between SNe stretches and LsSFR measurements, which trace progenitor age, using the SNF sample. This relation is shown in Fig. 4, and given the structure of the stretch-LsSFR scatter plot, our model of the underlying SNIa stretch distribution is defined as follows:

- for the young (i.e.,  $\log(\text{LsSFR}) > -10.82$ ) population, the underlying stretch distribution is modeled as a normal distribution  $N(\mu_1, \sigma_1^2)$ ;
- the old (i.e.,  $\log(\text{LsSFR}) < -10.82$ ) population stretch distribution is modeled as  $a \times N(\mu_1, \sigma_1^2) + (1-a) \times N(\mu_2, \sigma_2^2)$ , i.e. a Gaussian mixture where one mode is the same as the young population  $\alpha$ ,  $a$  representing the relative influence of the two Gaussians.

When combining our prediction of the evolution of young SNe Ia as a function of redshift (Eq. 1), and the stretch distribution of both young and old SNe Ia, our model for the underlying distribution of stretch  $X(z)$  as a function of redshift is:

$$X_1(z) = \delta(z) \times N(\mu_1, \sigma_1^2) + (1 - \delta(z)) \times [a \times N(\mu_1, \sigma_1^2) + (1 - a) \times N(\mu_2, \sigma_2^2)]. \quad (2)$$

The maximum-likelihood estimate of the 5 free parameters  $\theta \equiv (\mu_1, \mu_2, \sigma_1, \sigma_2, a)$  of the model is obtained by minimizing a pseudo- $\chi^2$   $\chi^2$  defined as:

$$\chi^2 = -2 \sum_i \ln \mathcal{P}(x_1^i | \theta; dx_1^i, y^i), \quad (3)$$

with

$$\begin{aligned} \mathcal{P}(x_1^i | \theta; dx_1^i, y^i) = & y^i \times N(x_1^i | \mu_1, \sigma_1^2 + dx_1^{i,2}) + \\ & (1 - y^i) \times [a \times N(x_1^i | \mu_1, \sigma_1^2 + dx_1^{i,2}) + \\ & (1 - a) \times N(x_1^i | \mu_2, \sigma_2^2 + dx_1^{i,2})] \end{aligned} \quad (4)$$

where  $i$  is the index of the SN Ia,  $x_1^i$ ,  $dx_1^i$  and  $y^i$  are the SALT2.4 stretch, its associated error and the probability that the SN is young, respectively. In practice, to ensure fraction  $a$  is constrained between 0 and 1, we fit for  $\alpha$  such that  $a = \arctan(\alpha)/\pi + 0.5$ , which results into asymmetric error on  $a$ .

Depending on whether  $y^i$  can be estimated directly from LsSFR measurements or not, there are two ways to proceed,

"which we now discuss"

#### 3.1.1. With LsSFR measurements

For the SNfactory sample, we can readily set  $y^i = p_y^i$ , the probability to have  $\log(\text{LsSFR}) \geq -10.82$  (see Fig. 4), to minimize Eq. 3 with respect to  $\theta$ . Results on fitting the SNf SNe with this model are shown Table 2 and illustrated in Fig. 4.

SNfactory

#### 3.1.2. Without LsSFR measurements

When lacking direct LsSFR measurements (i.e.  $p_y^i$ ), we can extend the analysis to non-SNfactory samples by using the redshift-evolution of the fraction  $\delta(z)$  of young SNe Ia (Eq. 1) as a proxy for the probability of a SN to be young. This still corresponds to minimizing Eq. 3 with respect to the parameters  $\theta \equiv (\mu_1, \mu_2, \sigma_1, \sigma_2, a)$  of the stretch distribution  $X_1$  (Eq. 2), but this time assuming  $y^i = \delta(z^i)$  for any given SN  $i$ .

For the rest of the analysis, we will therefore minimize Eq. 3 using  $p_y^i$  – the probability for the SN  $i$  to be young – when available (i.e. for SNf dataset), and  $\delta(z^i)$  – the expected fraction of young SNe Ia at the SN redshift  $z^i$  – otherwise.

Results on fitting this model on all the 569 (resp. 422) SNe from the fiducial (resp. conservative) sample are given Table 2 and illustrated in Fig. 5. We see in this figure that the measured mean SN Ia stretch per bin of redshift closely follows our redshift drift modeling; that is, when considering selection-bias-free SN Ia samples, SNe Ia at higher redshift have on average larger stretch ( $0.34 \pm 0.10$  at  $z \sim 0.65$ ) than those at lower redshift ( $-0.17 \pm 0.10$  at  $z \sim 0.05$ ). This is indeed what is expected if old environments favor low SN stretches (e.g. Howell et al. 2007) and if the fraction of old SNe Ia declines as a function of redshift. See section 4 for a more quantitative discussion.

for declines

#### 3.2. Alternative models

In section 3.1, we have modeled the underlying stretch distribution following Rigault et al. (2018), i.e. as a single Gaussian for the young SNe Ia and a mixture of two Gaussians for the old SNe Ia population, the same as the young-population one plus another for the fast declining SNe Ia that seem to only exist in old populations. This is our so-called "Base" model.

However, to test different modeling choices, we have implemented a suite of alternative parametrizations that we also adjust to the data following the procedure described section 3.1.2.

Howell et al. (2007) used a simpler model per age bin, assuming a normal distribution for both the young and the old population. We thus consider a "Howell+drift" model, with one single Gaussian per age group and the  $\delta(z)$  drift from (Rigault et al. 2018, see Eq. 1).

Alternatively, since we aim at probing the existence of a redshift drift, we are also testing non-drifting models by restricting the "Base" and "Howell" models to use a supposedly redshift-independent fraction  $\delta(z) = f$  of young SNe; these models are labeled "Base constant" and "Howell constant".

We are also considering other non-drifting models, notably the one developed for the Beam with Bias Correction (BBC, Scolnic & Kessler 2016; Kessler & Scolnic 2017), currently used in recent SN cosmological analyses (e.g. Scolnic et al. 2018; Abbott et al. 2019; Riess et al. 2016, 2019) to account for Malmquist biases. The BBC formalism assumes sample-based (hence intrinsically non-drifting) asymmetric Gaussian stretch distributions:  $N(\mu, \sigma_-^2 \text{ if } x_1 < \mu, \text{ else } \sigma_+^2)$ . The idea behind this sample-based approach is twofold: (1) Malmquist biases are driven by survey properties and (2) because current

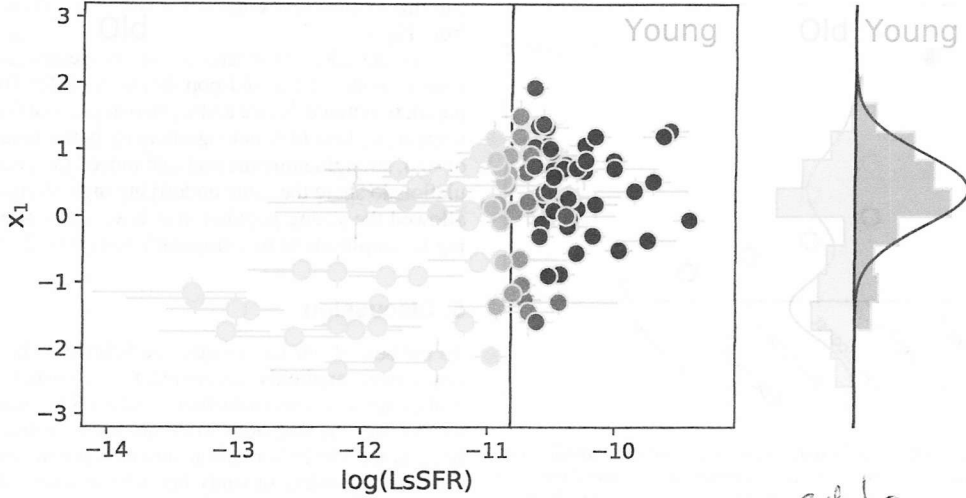


**Fig. 4.** Main: SALT2 .4 lightcurve stretch ( $x_1$ ) as a function of the local specific star formation rate (LsSFR) for SNf SNe used in this analysis. The color corresponds to the probability  $p_y$  for the SNe Ia to be young, i.e. to have  $\log \text{LsSFR} \geq -10.82$ ; see Rigault et al. (2018). Right: histogram of  $p_y$ -weighted distribution of the SN stretches. On both panels we illustrate the Base model fitted on the SNf SNe. The young and old population contributions are shown in purple and yellow, respectively.

**Table 2.** Best fit values of the parameters for the Base stretch distribution model when applied to the SNf dataset only (114 SNe Ia), the reference 569 SN Ia sample or the conservative one (422).

Sample	$\mu_1$	$\sigma_1$	$\mu_2$	$\sigma_2$	a
SNf	$0.41 \pm 0.08$	$0.55 \pm 0.06$	$-1.38 \pm 0.10$	$0.44 \pm 0.08$	$0.48^{+0.08}_{-0.08}$
Fiducial	$0.37 \pm 0.05$	$0.61 \pm 0.04$	$-1.22 \pm 0.16$	$0.56 \pm 0.10$	$0.51^{+0.09}_{-0.10}$
Conservative	$0.38 \pm 0.05$	$0.60 \pm 0.04$	$-1.26 \pm 0.13$	$0.53 \pm 0.08$	$0.47^{+0.09}_{-0.08}$

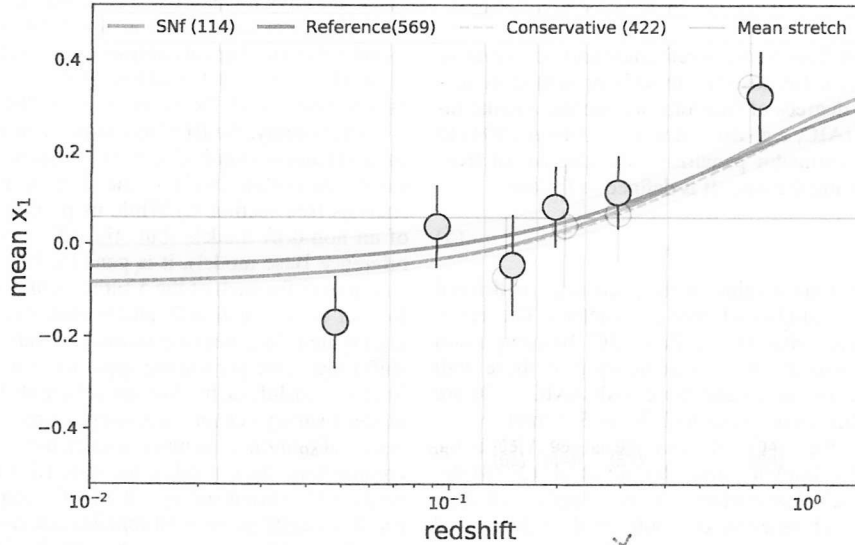


**Fig. 5.** Evolution of the mean SN SALT2 .4 stretch ( $x_1$ ) as a function of redshift. Markers show the mean stretch measured in redshift bins of equal sample size, indicated in light gray at the bottom of each redshift bins. Full and light markers are used when considering the fiducial or the conservative samples, respectively. The orange horizontal line represents the mean stretch of the reference sample, illustrating the expectation if the SN stretch distribution is not evolving with redshift. Best fits of our Base drifting model are shown as blue, dashed-blue and gray, when fitted on the fiducial sample, the conservative one or the SNf dataset only, respectively; all are compatible. The light-blue illustrates the amplitude of the error of the best fit model when considering the reference dataset.

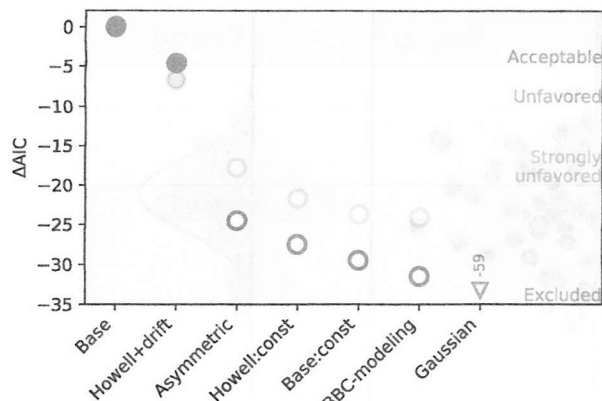


**Fig. 6.**  $\Delta\text{AIC}$  between “Base” model (reference) and other models (see Table 3). Full and open blue markers correspond to models with and without redshift drift, respectively. Light markers show the results when this analysis is performed on the conservative sample rather than the fiducial one. Color-bands illustrate the validity of the models, from Acceptable ( $\Delta\text{AIC} > -5$ ) to Excluded ( $\Delta\text{AIC} < -20$ ); see text. According to the AIC, all non-drifting models (open symbols) are excluded to be as good representation of the data in comparison to our Base (drifting) model.

surveys cover limited redshift ranges, doing so covers some potential redshift evolution information (Scolnic & Kessler 2016; Scolnic et al. 2018). See further discussion concerning the BBC in section 5.2.

Finally, for the sake of completeness, we also consider simple “Gaussian” and “asymmetric” Gaussian non-drifting models.

## 4. Results

We applied each model on both the reference and conservative samples (cf. section 2). Because the models presented in section 3 have different degrees of freedom, we use the Akaike Information Criterion (AIC, e.g. Burnham & Anderson 2004) to compare them. This estimator penalizes extra degrees of freedom to avoid over-fitting the data. It is defined as follow:

$$\text{AIC} = \chi^2_{\min} + 2k \quad (5)$$

where  $\chi^2_{\min}$  is the minimum value of the pseudo- $\chi^2$  as defined Eq. (3) and  $k$  is the number of free parameters. The reference model is the one with the smallest AIC. In comparison to this model, those with  $\Delta\text{AIC} < 5$  are acceptable, those with  $5 < \Delta\text{AIC} < 10$  are unfavored and those with  $\Delta\text{AIC} > 20$  are excluded. This roughly corresponds to 2, 3 and 5  $\sigma$  limits.

We first note that the best model (with smallest AIC) is the so-called Base model, implementing Rigault et al. (2018) description of the stretch distribution and its redshift evolution. This is therefore the reference model, both on the fiducial and conservative samples.

Furthermore, we find that underlying stretch distributions not including a redshift drift are all excluded to describe the data as well as the Base model. In fact, the best non-drifting model (Asymmetric) has a very marginal chance ( $p \equiv \exp(\Delta\text{AIC}/2) = 5 \times 10^{-6}$ ) to describe the data as well as the Base model. This result is just a quantitative assessment of qualitative facts clearly visible in Fig. 5: the mean SN stretch per bin of redshift strongly suggests a redshift evolution rather than having a constant value,

and this evolution is compatible with the redshift drift expected from Eq. 1.

For the sake of robustness, we also tested to leave the high-stretch mode of the old-population to differ from the young-population mode, hence adding two degrees of freedom. The corresponding best fit is not significantly better resulting to a  $\Delta\text{AIC}$  of -0.4, strengthening the fact that indeed the young and old population do share the same underlying high-stretch mode. We also allowed the young population to have a low-stretch mode, finding its amplitude to be compatible with 0 (< 2%).

## 5. Discussion

To the best of our knowledge, the SNIa stretch redshift drift has never been explicitly accounted for in cosmological analyses. Not doing so is a second order issue for SN cosmology as it only affects the way one does Malmquist bias correction. Indeed, as long as the Phillip’s relation standardization parameter  $\alpha$  is not redshift dependent (a study behind the scope of this paper, but see e.g. Scolnic et al. 2018), if a sample is free from selection effects, the stretch-corrected SNe Ia magnitudes used for cosmology are blind to the underlying stretch distribution. Yet, modern surveys do have significant Malmquist bias at least for the upper half of their SN redshift distribution. Then, an ill-modelling of the underlying stretch distribution will bias the derived SN magnitude for these (see e.g., Rubin et al. 2015; Rubin & Hayden 2016). The fact that the currently used stretch modeling for Malmquist bias correction in SN cosmology (BBC) is excluded to be an as good description of the data than our drifting model is worrisome and we further discussed in the next sections.

### 5.1. BBC formalism and underlying stretch distributions

The state-of-the-art tool for doing Malmquist bias correction in SN cosmology is the BBC formalism described in Scolnic & Kessler (2016) and Kessler & Scolnic (2017), which is used in recent SN cosmological analyses (Jones et al. 2018; Scolnic et al. 2018; Brout et al. 2019; Abbott et al. 2019) including the direct measurement of  $H_0$  (Riess et al. 2016, 2019).

Surprisingly, the BBC technique, which assumes an individual asymmetric distribution per sample (Scolnic & Kessler 2016; Kessler & Scolnic 2017), is one of the worst modelisation in our analysis (see section 4.) While its pseudo- $\chi^2$ ,  $\chi^2$ , is the smallest of all non-drift models (but still  $\Delta\chi^2 = -11.5$  worse than the reference Base model), it is penalized by requiring 15 free parameters (3 for each of the 5 samples of the analysis). Scolnic & Kessler (2016, section 2) and Scolnic et al. (2018, section 5.4) highlighted that, because traditional surveys span limited redshift ranges, the per sample approach can somewhat account for implicit redshift drifts. We stress here that, as measurements of modern surveys cover increasingly larger redshift ranges to reduce calibration systematic uncertainties, this approach is becoming less valid, notably for PS1, DES and, soon, LSST. Already with current surveys, the BBC sample-based technique is ruled out to be as good representation of the data as our best model ( $\Delta\text{AIC} < -20$ ), which could be interpreted as a probability  $p = 2 \times 10^{-7}$  to be an as good representation of the data as the Base model. Remark that considering the SNF dataset like any other (i.e. ignoring the LSSFR information see section 3), reduces this difference to  $\Delta\text{AIC} < -10$ , still strongly unfavoring the modeling currently used as part of the BBC Malmquist bias correction.

We report in Table 4 the samples’  $\sigma_{\pm}$  and  $\mu_0$  fitted on the supposedly selection-free samples using our fiducial cuts (see

**Table 3.** Comparison of the relative ability for a model to describe the data. For each considered model, we report if the model is drifting or not, its number of free parameters and, for both the fiducial and the conservative cuts, the pseudo  $\chi^2$ ,  $X^2$  (see Eq. 3) the AIC and the AIC difference ( $\Delta\text{AIC}$ ) between this model and the Base model used as reference for its has the lowest AIC.

Name	drift	$k$	Fiducial sample (569 SNe)			Conservative sample (422 SNe)		
			$\chi^2$	AIC	$\Delta\text{AIC}$	$X^2$	AIC	$\Delta\text{AIC}$
Base	$\delta(z)$	5	1456.7	1466.7	–	1079.5	1089.5	–
Howell+drift	$\delta(z)$	4	1463.3	1471.3	-4.6	1088.2	1096.2	-6.7
Asymmetric	–	3	1485.2	1491.2	-24.5	1101.3	1107.3	-17.8
Howell:const	$f$	5	1484.2	1494.2	-27.5	1101.2	1111.2	-21.7
Base:const	$f$	6	1484.2	1496.2	-29.5	1101.2	1113.2	-23.7
BBC	per sample	3x5	1468.2	1498.2	-31.5	1083.6	1113.6	-24.1
Gaussian	–	2	1521.8	1525.8	-59.1	1142.6	1146.6	-57.1

**Table 4.** Best-fit parameters for our sample-based asymmetric modeling of the underlying stretch distribution.

Asymmetric	$\sigma_-$	$\sigma_+$	$\mu_0$
SNf	$1.34 \pm 0.13$	$0.41 \pm 0.10$	$0.68 \pm 0.15$
SDSS	$1.31 \pm 0.11$	$0.42 \pm 0.09$	$0.72 \pm 0.13$
PS1	$1.01 \pm 0.11$	$0.52 \pm 0.12$	$0.38 \pm 0.16$
SNLS	$1.41 \pm 0.13$	$0.15 \pm 0.13$	$1.22 \pm 0.15$
HST	$0.76 \pm 0.36$	$0.79 \pm 0.35$	$0.11 \pm 0.44$

section 2. We find our results in close agreement with Scolnic & Kessler (2016) for SNLS and SDSS and with Scolnic et al. (2018) for PS1, who derived these model parameters using the full BBC formalism, using numerous simulations to model the selection effects (see details e.g., section 3 of Kessler & Scolnic 2017). The agreement between our fit of the asymmetric gaussians on the supposedly selection-free part of the samples and the results derived using the BBC formalism support that our sample selection indeed enables to get a sample with negligible selection effects. If we were to use Scolnic & Kessler (2016) and Scolnic et al. (2018) best fit values for SNLS, SDSS and PS1, respectively, the  $\Delta\text{AIC}$  between our Base drifting model and the BBC modeling would go even deeper from -32 to -47.

### 5.2. First step toward quantification of the cosmological impact of inaccurate stretch distribution modeling.

We illustrate in Fig. 7 the prediction difference in the underlying stretch distribution between the BBC modeling and our Base drifting model for the PS1 sample. Our model is bimodal and the relative amplitude of each mode depends on the redshift-dependent fraction of old SNe Ia in the sample: the higher the fraction of old SNe Ia (lower redshift), the higher the amplitude of the low-stretch mode. This redshift dependency is shown as blue to red underlying distributions in Fig. 7 for redshift ranges covered by PS1. The observed  $x_1$  histogram corresponds to the sum of individual SN-redshift underlying distributions. As expected, the two approaches strongly differ in modeling the negative part of the SN stretch distribution. The BBC asymmetric distribution goes in the middle of the bimodal distribution, over-estimating the number of SNe Ia at  $x_1 \sim -0.7$  and under-estimating it at  $x_1 \sim -1.7$  for typical PS1 SN redshifts. This means that the bias-correction of individual SN stretch  $\delta_{x_1}$  (Kessler & Scolnic 2017) and consequently the magnitude bias

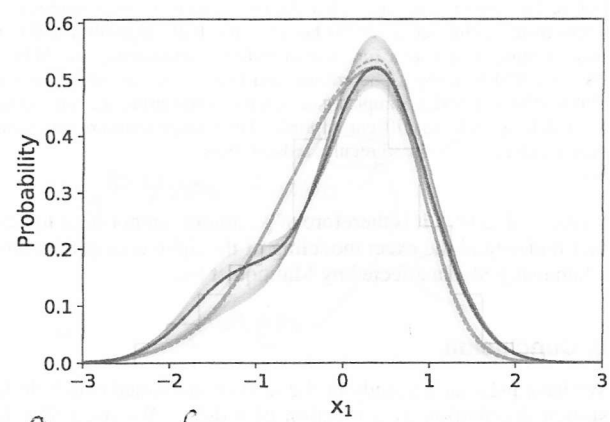


**Fig. 7.** Distribution of the PS1 SNIa SALT2.4 stretch ( $x_1$ ) after the fiducial redshift limit cut (grey histogram). This distribution is supposed to be random drawing of the underlying stretch distribution. The green line shows the BBC modeling of this underlying distribution (asymmetric Gaussian). The full line (band) is our best fit (its error); the dashed line shows Scolnic et al. (2018) result. The black line (band) show our best fitted Base-modeling (its error, see Table XX) that includes redshift drift. For illustration, we show as colored (from blue to red with increasing redshifts) the evolution of the underlying stretch distribution as a function of redshift for the redshift range covered by PS1 data.

correction  $\mu_B$  is most likely inaccurate and this inaccuracy is redshift dependent

The amplitude of this bias for cosmology is beyond the scope of this paper given the complexity of the BBC analysis. It would require a full study using our Base model given Eq. 2 in place of the sample-based asymmetric modeling as part of the BBC simulations.

Nonetheless, it is interesting to study the expected mean stretch difference as a function of redshift when considering that the underlying SN stretch distribution follows either the BBC formalism or our Base drifting modeling. This is shown Fig. 8, where, for clarity we convert this difference in magnitude using  $\alpha = 0.156$  (Scolnic et al. 2018).

We see in this figure that the amplitude of modeling difference is a few tens of millimag, which corresponds to the expected bias affecting SNeIa affected by sample selection effects. For comparison, the amplitude of this effect is similar in scale to the expected effect of exotic forms of dark energy could have on  $\mu(z)$ . Consequently, in the era of modern cosmology, where we aim at probing  $w_0$  at a sub-percent and  $w_a$  at a few percent (e.g.,

reward

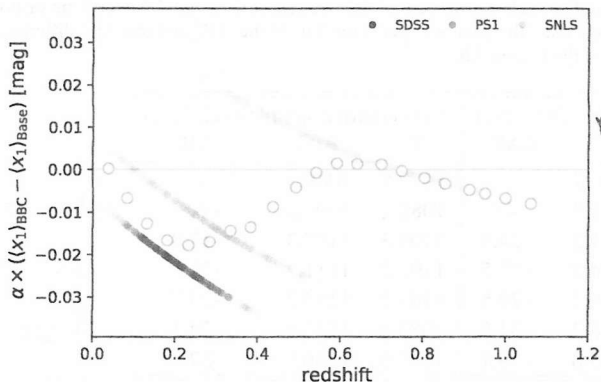


**Fig. 8.** Difference of mean stretch standardization (in mag, using  $\alpha = 0.156$  from Scolnic et al. 2018) between the BBC algorithm and our Base drifting model as a function of redshift, considering the SDSS, PS1 and SNLS dataset. The colored markers show the difference for SDSS, PS1 and SNLS samples (see legend) considering the individual SN redshifts (no redshift cut applied). The orange markers represent their mean evolution in 30 regular redshift bins.

Ivezic et al. 2019), it is therefore of paramount importance to further understand the exact modeling of the lightcurve parameters when using SNeIa affected by Malmquist bias.

## 6. Conclusion

We have presented a study of the drift of the underlying SNe Ia stretch distribution as a function of redshift. We used SNe Ia from magnitude-limited surveys from the Pantheon dataset (Scolnic et al. 2018, SDSS, PS1 and SNLS) as well as HST, to which we added SNfactory data from Rigault et al. (2018) for the low-redshift bin. We only considered the supernovae that have been discovered in redshift ranges of each surveys where selection effects are negligible. This way the observed SNe Ia stretch are random sampling of the true underlying distribution. This corresponds to 569 SNe Ia (422 when considering more conservative cuts).

Following observations made in Rigault et al. (2018), we introduced a redshift drift modeling which depends on the expected fraction of young and old SNe Ia as a function of redshift, each age-population having its own underlying stretch distribution. We have studied various suites of distributions, including non-drifting modeling. We also studied the stretch distribution modeling of the current version of the BBC Malmquist bias correction algorithm used by recent SNeIa cosmological analyses.

Our conclusions are the following:

1. Non-drifting models are excluded to be as good descriptions of the data our Base model. This model assumes that: (1) the young population has a unimodal Gaussian stretch distribution while the old population stretch one is bimodal, one mode being the young one; (2) the evolution of the relative fraction of young and old SNe Ia follows the prediction made in Rigault et al. (2018).
2. Given 1., we conclude that the SNe Ia stretch is indeed drifting, as already suggested by e.g. Howell et al. (2007).
3. The BBC approach, which assumes each survey to have its own asymmetric Gaussian distribution, is excluded to be an as good description of the data as our drifting model. Hence, the BBC sample-based approach does not accurately account

for redshift drift unlike what was suggested by Scolnic & Kessler (2016) and Scolnic et al. (2018).

4. An inaccurate underlying stretch distribution modeling is estimated to bias to the order of a few percents the mean standardized magnitude of SNe Ia affected selection effects. This is comparable in scale to the observational signature of exotic forms of dark energy and is therefore a significant source of systematic that should be carefully studied.

5. We suggest to use the following stretch population modeling:

$$X_1(z) = \delta(z) \times N(\mu_1, \sigma_1^2) + (1 - \delta(z)) \times [a \times N(\mu_1, \sigma_1^2) + (1 - a) \times N(\mu_2, \sigma_2^2)] \quad (6)$$

with:  $a = 0.51$ ,  $\mu_1 = 0.37$ ,  $\mu_2 = -1.22$ ,  $\sigma_1 = 0.61$ ,  $\sigma_2 = 0.56$  (see Table 2) and using the age-population drift modelization  $\delta(z)$  defined in Rigault et al. (2018) with  $K = 0.87$ :

$$\delta(z) = (K^{-1} \times (1+z)^{-2.8} + 1)^{-1}. \quad (7)$$

*Acknowledgements.* This project has received funding from the European Research Council (ERC) under the European Union's Horizon 2020 research and innovation programme (grant agreement n° 759194 - USNAC).

## Acknowledgements?

### References

- Abbott, T. M. C., Abdalla, F. B., Alarcon, A., et al. 2018, Phys. Rev. D, 98, 043526  
 Abbott, T. M. C., Allam, S., Andersen, P., et al. 2019, ApJ, 872, L30  
 Aldering, G. 2004, APS April Meeting Abstracts 2004, V4.003  
 Astier, P., Guy, J., Regnault, N., et al. 2006, A&A, 447, 31  
 Ata, M., Kitaura, F.-S., Chuang, C.-H., et al. 2017, MNRAS, 467, 3993  
 Aubourg, É., Tojeiro, R., Jimenez, R., et al. 2008, A&A, 492, 631  
 Bazin, G., Ruhlmann-Kleider, V., Palanque-Delabrouille, N., et al. 2011, A&A, 534, A43  
 Bellm, E. C., Kulkarni, S. R., Graham, M. J., et al. 2019, PASP, 131, 018002  
 Betoule, M., Kessler, R., Guy, J., et al. 2014, A&A, 568, A22  
 Brout, D., Scolnic, D., Kessler, R., et al. 2019, ApJ, 874, 150  
 Burnham, K., Anderson, D., 2004, Sociological Methods & Research, 33, 2  
 Campbell, H., D'Andrea, C. B., Nichol, R. C., et al. 2013, ApJ, 763, 88  
 Chabanier, S., Millea, M., & Palanque-Delabrouille, N. 2019, MNRAS, 489, 2247  
 Childress, M., Aldering, G., Antilogus, P., et al. 2013, ApJ, 770, 108  
 Childress, M. J., Wolf, C., & Zahid, H. J. 2014, MNRAS, 445, 1898  
 Coles, P., & Jones, B. 1991, MNRAS, 248, 1  
 D'Andrea, C. B., Gupta, R. R., Sako, M., et al. 2011, ApJ, 743, 172  
 Dilday, B., Kessler, R., Frieman, J. A., et al. 2008, ApJ, 682, 262  
 Feeney, S. M., Peiris, H. V., Williamson, A. R., et al. 2019, Phys. Rev. Lett., 122, 061105  
 Freedman, W. L., Madore, B. F., Hatt, D., et al. 2019, ApJ, 882, 34  
 Freedman, W. L., Madore, B. F., Hoyt, T., et al. 2020, arXiv e-prints, arXiv:2002.01550  
 Frieman, J. A., Bassett, B., Becker, A., et al. 2008, AJ, 135, 338  
 Graham, M. J., Kulkarni, S. R., Bellm, E. C., et al. 2019, PASP, 131, 078001  
 Gupta, R. R., D'Andrea, C. B., Sako, M., et al. 2011, ApJ, 740, 92  
 Guy, J., Astier, P., Baumont, S., et al. 2007, A&A, 466, 11  
 Hamuy, M., Phillips, M. M., Suntzeff, N. B., et al. 1996, AJ, 112, 2391  
 Hamuy, M., Trager, S. C., Pinto, P. A., et al. 2000, AJ, 120, 1479  
 Howell, D. A., Sullivan, M., Conley, A., et al. 2007, ApJ, 667, L37  
 Ivezic, Ž., Kahn, S. M., Tyson, J. A., et al. 2019, ApJ, 873, 111  
 Jones, D. O., Riess, A. G., & Scolnic, D. M. 2015, ApJ, 812, 31  
 Jones, D. O., Riess, A. G., Scolnic, D. M., et al. 2018, ApJ, 867, 108  
 Jones, D. O., Scolnic, D. M., Riess, A. G., et al. 2018, ApJ, 857, 51  
 Jones, D. O., Scolnic, D. M., Foley, R. J., et al. 2019, ApJ, 881, 19  
 Kelly, P. L., Hicken, M., Burke, D. L., et al. 2010, ApJ, 715, 743  
 Kessler, R., Becker, A. C., Cinabro, D., et al. 2009, ApJS, 185, 32  
 Kessler, R., & Scolnic, D. 2017, ApJ, 836, 56  
 Kim, Y.-L., Smith, M., Sullivan, M., et al. 2018, ApJ, 854, 24  
 Kim, Y.-L., Kang, Y., & Lee, Y.-W. 2019, Journal of Korean Astronomical Society, 52, 181  
 Knox, L., & Millea, M. 2019, arXiv e-prints, arXiv:1908.03663  
 Lampeitl, H., Smith, M., Nichol, R. C., et al. 2010, ApJ, 722, 566  
 Mannucci, F., Della Valle, M., Panagia, N., et al. 2005, A&A, 433, 807  
 Mannucci, F., Della Valle, M., & Panagia, N. 2006, MNRAS, 370, 773

Unclear whether all these are used

- Maoz, D., Mannucci, F., & Nelemans, G. 2014, ARA&A, 52, 107  
Neill, J. D., Sullivan, M., Balam, D., et al. 2006, AJ, 132, 1126  
Neill, J. D., Sullivan, M., Howell, D. A., et al. 2009, ApJ, 707, 1449  
Pan, Y.-C., Sullivan, M., Maguire, K., et al. 2014, MNRAS, 438, 1391  
Perlmutter, S., Aldering, G., Goldhaber, G., et al. 1999, ApJ, 517, 565  
Perrett, K., Balam, D., Sullivan, M., et al. 2010, AJ, 140, 518  
Planck Collaboration, Ade, P. A. R., Aghanim, N., et al. 2016, A&A, 594, A13  
Poulin, V., Smith, T. L., Karwal, T., et al. 2019, Phys. Rev. Lett., 122, 221301  
Planck Collaboration, Aghanim, N., Akrami, Y., et al. 2018, arXiv e-prints, arXiv:1807.06209  
Reid, M. J., Pesce, D. W., & Riess, A. G. 2019, arXiv e-prints, arXiv:1908.05625  
Rest, A., Scolnic, D., Foley, R. J., et al. 2014, ApJ, 795, 44  
Riess, A. G., Filippenko, A. V., Challis, P., et al. 1998, AJ, 116, 1009  
Riess, A. G., Macri, L., Casertano, S., et al. 2009, ApJ, 699, 539  
Riess, A. G., Macri, L. M., Hoffmann, S. L., et al. 2016, ApJ, 826, 56  
Riess, A. G., Casertano, S., Yuan, W., et al. 2018, ApJ, 861, 126  
Riess, A. G., Casertano, S., Yuan, W., et al. 2019, ApJ, 876, 85  
Rigault, M., Copin, Y., Aldering, G., et al. 2013, A&A, 560, A66  
Rigault, M., Aldering, G., Kowalski, M., et al. 2015, ApJ, 802, 20  
Rigault, M., Brinnel, V., Aldering, G., et al. 2018, arXiv:1806.03849  
Rodney, S. A., Riess, A. G., Strolger, L.-G., et al. 2014, AJ, 148, 13  
Roman, M., Hardin, D., Betoule, M., et al. 2018, A&A, 615, A68  
Rose, B. M., Garnavich, P. M., & Berg, M. A. 2019, ApJ, 874, 32  
Rubin, D., Aldering, G., Barbary, K., et al. 2015, ApJ, 813, 137  
Rubin, D., & Hayden, B. 2016, ApJ, 833, L30  
Sako, M., Bassett, B., Becker, A., et al. 2008, AJ, 135, 348  
Scannapieco, E., & Bildsten, L. 2005, ApJ, 629, L85  
Scolnic, D., Rest, A., Riess, A., et al. 2014, ApJ, 795, 45  
Scolnic, D., & Kessler, R. 2016, ApJ, 822, L35  
Scolnic, D. M., Jones, D. O., Rest, A., et al. 2018a, ApJ, 859, 101  
Scolnic, D. M., Lochner, M., Gris, P., et al. 2018, arXiv e-prints, arXiv:1812.00516  
Scolnic, D., Perlmutter, S., Aldering, G., et al. 2019, Astro2020: Decadal Survey on Astronomy and Astrophysics, 2020, 270  
Strolger, L.-G., Riess, A. G., Dahlen, T., et al. 2004, ApJ, 613, 200  
Sullivan, M., Le Borgne, D., Pritchett, C. J., et al. 2006, ApJ, 648, 868  
Sullivan, M., Conley, A., Howell, D. A., et al. 2010, MNRAS, 406, 782  
Tasca, L. A. M., Le Fèvre, O., Hathi, N. P., et al. 2015, A&A, 581, A54  
Wiseman, P., Smith, M., Childress, M., et al. 2020, arXiv e-prints, arXiv:2001.02640  
Wong, K. C., Suyu, S. H., Chen, G. C.-F., et al. 2019, arXiv e-prints, arXiv:1907.04869

